

Polymorphic residues in rice NLRs expand binding and response to effectors of the blast pathogen

Juan Carlos De la Concepcion ^{1,6}, Marina Franceschetti ^{1,6}, Abbas Maqbool ¹,
Hiromasa Saitoh ², Ryohei Terauchi ^{3,4}, Sophien Kamoun ⁵ and Mark J. Banfield ^{1*}

Accelerated adaptive evolution is a hallmark of plant–pathogen interactions. Plant intracellular immune receptors (NLRs) often occur as allelic series with differential pathogen specificities. The determinants of this specificity remain largely unknown. Here, we unravelled the biophysical and structural basis of expanded specificity in the allelic rice NLR Pik, which responds to the effector AVR-Pik from the rice blast pathogen *Magnaporthe oryzae*. Rice plants expressing the *Pikm* allele resist infection by blast strains expressing any of three AVR-Pik effector variants, whereas those expressing *Pikp* only respond to one. Unlike *Pikp*, the integrated heavy metal-associated (HMA) domain of *Pikm* binds with high affinity to each of the three recognized effector variants, and variation at binding interfaces between effectors and *Pikp*-HMA or *Pikm*-HMA domains encodes specificity. By understanding how co-evolution has shaped the response profile of an allelic NLR, we highlight how natural selection drove the emergence of new receptor specificities. This work has implications for the engineering of NLRs with improved utility in agriculture.

The innate immune systems of plants and animals monitor the extracellular space and the intracellular environment for the presence and activities of microbial pathogens^{1,2}. In plants, immune receptors of the NLR (nucleotide-binding, leucine-rich repeat (LRR)) superfamily monitor the intracellular space for signatures of non-self, typically detecting translocated pathogen effector proteins either by direct binding or indirectly via monitoring their activity on host targets^{3,4}. Co-evolution between pathogens and hosts has driven the diversification of plant NLRs, with many NLR genes present in allelic series, with distinct effector recognition profiles^{5–15}. Pathogen effectors can show strong signatures of positive selection, including high levels of non-synonymous (resulting in amino acid changes) over synonymous polymorphisms^{5,7,12,16–18}. How NLR and effector diversification contributes to gene-for-gene immunity in plants is poorly understood. Defining how allelic NLRs recognize and respond to specific pathogen effectors offers new opportunities to engineer the control of plant diseases^{19,20}, leading to improved global food security.

Many NLRs function synergistically, with some acting as ‘sensors’, to detect pathogens, and others as ‘helpers’, which are required for the initiation of immunity^{1,21,22}. These NLRs can be genetically linked in pairs, with a shared promoter^{21,23–26}, or unlinked but part of a complex genetic network²⁷. One mechanism of effector recognition by sensor NLRs is via unconventional integrated domains that probably have their evolutionary origin as host effector targets^{28–31}. Such integrated domains can act as ‘baits’ to target effectors by direct binding or act as substrates of an effector’s enzymatic activity^{28,31}. Genetically paired NLRs with integrated domains have repeatedly evolved in rice^{29,30} and can detect effectors from the rice blast pathogen *Magnaporthe oryzae* (also known as *Pyricularia oryzae*), the causative agent of the most devastating disease of rice, which is the staple crop that feeds more than half of the world population^{5,25,26,32}.

The rice NLR pair *Pik* comprises *Pik*-1 (the sensor) and *Pik*-2 (the helper). This receptor pair responds to the *M. oryzae* effector AVR-Pik by direct binding to an integrated heavy metal-associated (HMA) domain, positioned between the coiled-coil and the nucleotide-binding domains of *Pik*-1³³ (Fig. 1a). Both the AVR-Pik effectors and the *Pik* NLRs exist as an allelic series in *M. oryzae* and rice, respectively, that most likely arose through co-evolutionary dynamics between pathogen and host^{5,34,35}. As such, they represent an excellent system for understanding the mechanistic basis of recognition in plant immunity. A comparison of amino acid sequence identity between the domains of paired *Pik* NLR alleles shows that the integrated HMA domain is the most polymorphic region³⁵ (Fig. 1a,c), which is consistent with this being the direct binding region for the AVR-Pik effectors. The HMA domain also contains variable amino acids that have been used as markers for *Pik* allele identification in rice³⁵. In addition, AVR-Pik is a remarkable example of an effector with an extreme signature of positive selection, as all known AVR-Pik nucleotide polymorphisms are non-synonymous, resulting in amino acid changes^{16,18} (Fig. 1b). Furthermore, these polymorphisms map to interface residues identified in the crystal structure of the effector variant AVR-PikD bound to the HMA domain of the NLR allele *Pikp*³³, suggesting that they are adaptive.

Although rice plants expressing the NLR allele *Pikp* are resistant to *M. oryzae* strains expressing the effector variant AVR-PikD, rice plants expressing the allele *Pikm* respond to strains expressing AVR-PikD, AVR-PikE or AVR-PikA³⁴ (Fig. 1b). Importantly, neither *Pikp* nor *Pikm* respond to the stealthy effector variant AVR-PikC, which evades detection by any known *Pik* NLR³⁴. The molecular mechanism by which *Pik* NLR variation acts to expand effector recognition remains unclear.

Previous work established the structural basis of AVR-PikD recognition by the *Pikp*-1 NLR³³. Here, we reveal how co-evolutionary

¹Department of Biological Chemistry, John Innes Centre, Norwich Research Park, Norwich, UK. ²Laboratory of Plant Symbiotic and Parasitic Microbes, Department of Molecular Microbiology, Faculty of Life Sciences, Tokyo University of Agriculture, Tokyo, Japan. ³Division of Genomics and Breeding, Iwate Biotechnology Research Center, Iwate, Japan. ⁴Laboratory of Crop Evolution, Graduate School of Agriculture, Kyoto University, Kyoto, Japan. ⁵The Sainsbury Laboratory, Norwich Research Park, Norwich, UK. ⁶These authors contributed equally: De la Concepcion, J. C. and Franceschetti, M. *e-mail: mark.banfield@jic.ac.uk

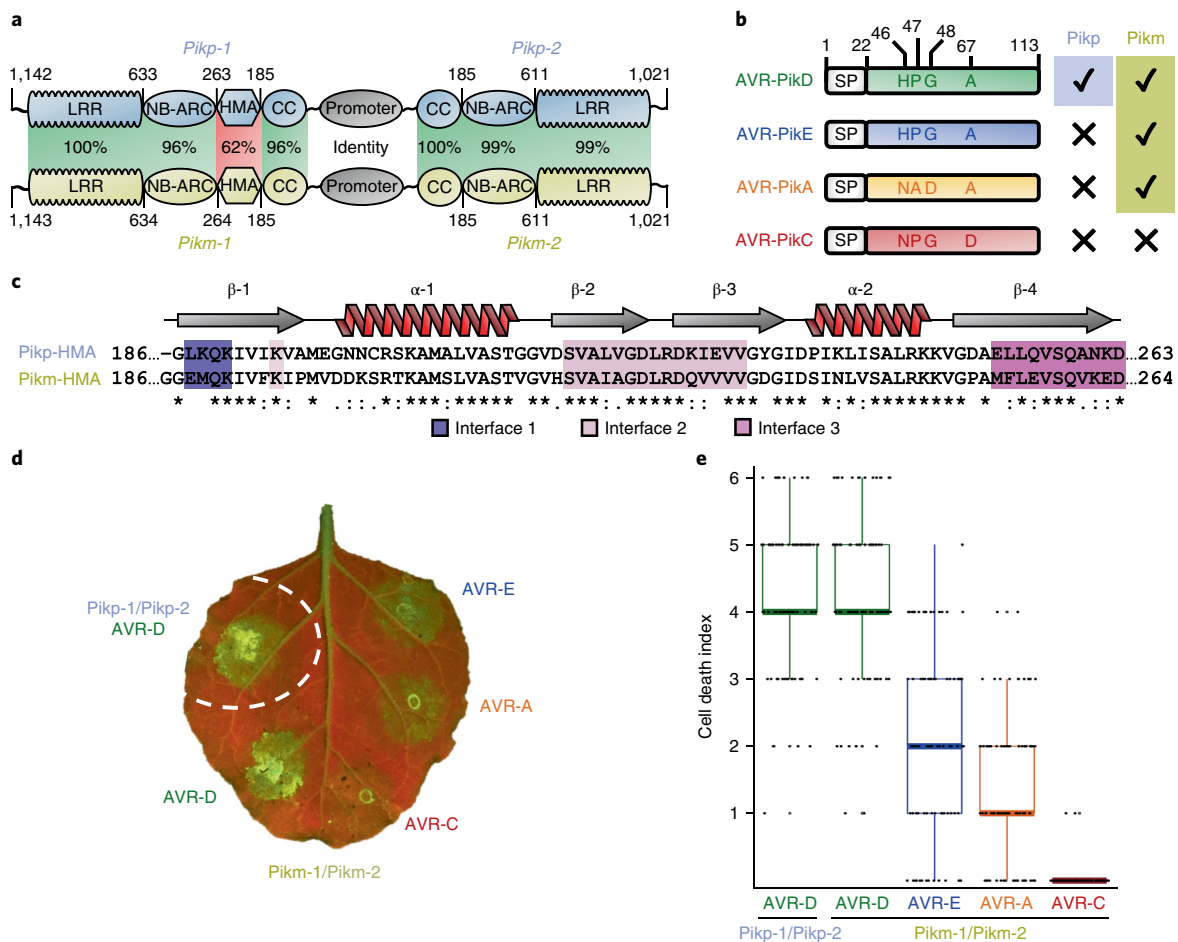


Fig. 1 | The Pikm-mediated cell death response to AVR-Pik effector variants in *N. benthamiana* phenocopies the Pikm resistance profile in rice.

a, Schematic representations of Pik NLR alleles. The sensor NLR (*Pik-1*) and the helper NLR (*Pik-2*) share a common promoter and the same overall domain architecture. *Pikp-1* and *Pikp-2* are shown on the top and *Pikm-1* and *Pikm-2* are shown on the bottom. Pairwise protein sequence identity between each domain is indicated, highlighting the diversification of the integrated HMA domain. CC, coiled coil domain; NB-ARC, nucleotide-binding domain. **b**, Schematic representations of AVR-Pik variants with amino acid polymorphisms shown (single-letter code), along with their *Pikp*-mediated or *Pikm*-mediated response profiles in rice (right)³⁴. SP, signal peptide. **c**, Amino acid sequence alignment of *Pikp-1* and *Pikm-1* HMA domains. Secondary structure features of the HMA fold are shown above, and the residues located to the interfaces described in the text and in Fig. 3 are highlighted. **d**, A representative leaf image showing *Pikm*-mediated cell death to AVR-Pik variants as autofluorescence under UV light; *Pikm*-mediated cell death with AVR-PikD is included as a positive control (surrounded by the dashed circle; no *Pikm-1/Pikm-2* was in this spot). **e**, Box plots showing repeats of the cell death assay. For each sample, the number of repeats was 90. The centre line represents the median, the box limits are the upper and lower quartiles, the whiskers are the 1.5× interquartile range and all of the data points are represented as dots. The cell death scoring scale used is shown in Supplementary Fig. 1d. For brevity, the effectors are labelled without the ‘Pik’ designation in panels **d** and **e** and, where appropriate, in Figs. 2–6.

dynamics between a pathogen and a host has driven the emergence of new receptor specificities. By taking advantage of our ability to reconstruct complexes between *Pik*-HMA domains and AVR-*Pik* effectors, and to recapitulate cell death responses (indicative of immunity) in the model plant *Nicotiana benthamiana*, we show a correlation between protein-binding affinities and the activation of immunity. By obtaining crystal structures of the *Pikm*-HMA domain (henceforth *Pikm*-HMA) in complex with three different AVR-*Pik* variants, we define the interfaces that support expanded effector recognition. We also obtained new structures of the *Pikp*-HMA domain (henceforth *Pikp*-HMA) in complex with the recognized effector AVR-*PikD*, but also with the unrecognized AVR-*PikE*. Together, these structures establish a previously unappreciated role for the carboxy terminus of the HMA domain in mediating effector interaction. Understanding how host NLRs have evolved new specificities in response to pathogen effectors highlights the potential to engineer new-to-nature receptors with improved functions, such as

recognition of stealthy effector variants, and has broad implications for rational design of plant NLRs.

Results

***Pikm*-mediated cell death in *N. benthamiana* recapitulates allele-specific effector responses in rice.** *Pikp*-mediated cell death in *N. benthamiana* phenocopies effector variant-specific resistance in rice, with *Pikp* responding to AVR-*PikD*, but not to AVR-*PikE*, AVR-*PikA* or AVR-*PikC*³³. Here, we show that *Pikm* responds to each of AVR-*PikD*, AVR-*PikE* or AVR-*PikA*, but not to AVR-*PikC*, in this assay (Fig. 1d,e and Table 1). These results match the response of rice cultivars expressing *Pikm* to *M. oryzae* strains encoding the effectors³⁴. Interestingly, we observe a qualitative hierarchy in the level of *Pikm*-mediated cell death in response to the effectors in the order AVR-*PikD* > AVR-*PikE* > AVR-*PikA* (Fig. 1d,e). To allow for direct comparison, we repeated this assay using the *Pikp* NLRs and the effector variants in the same expression vectors. We obtained equivalent results to those

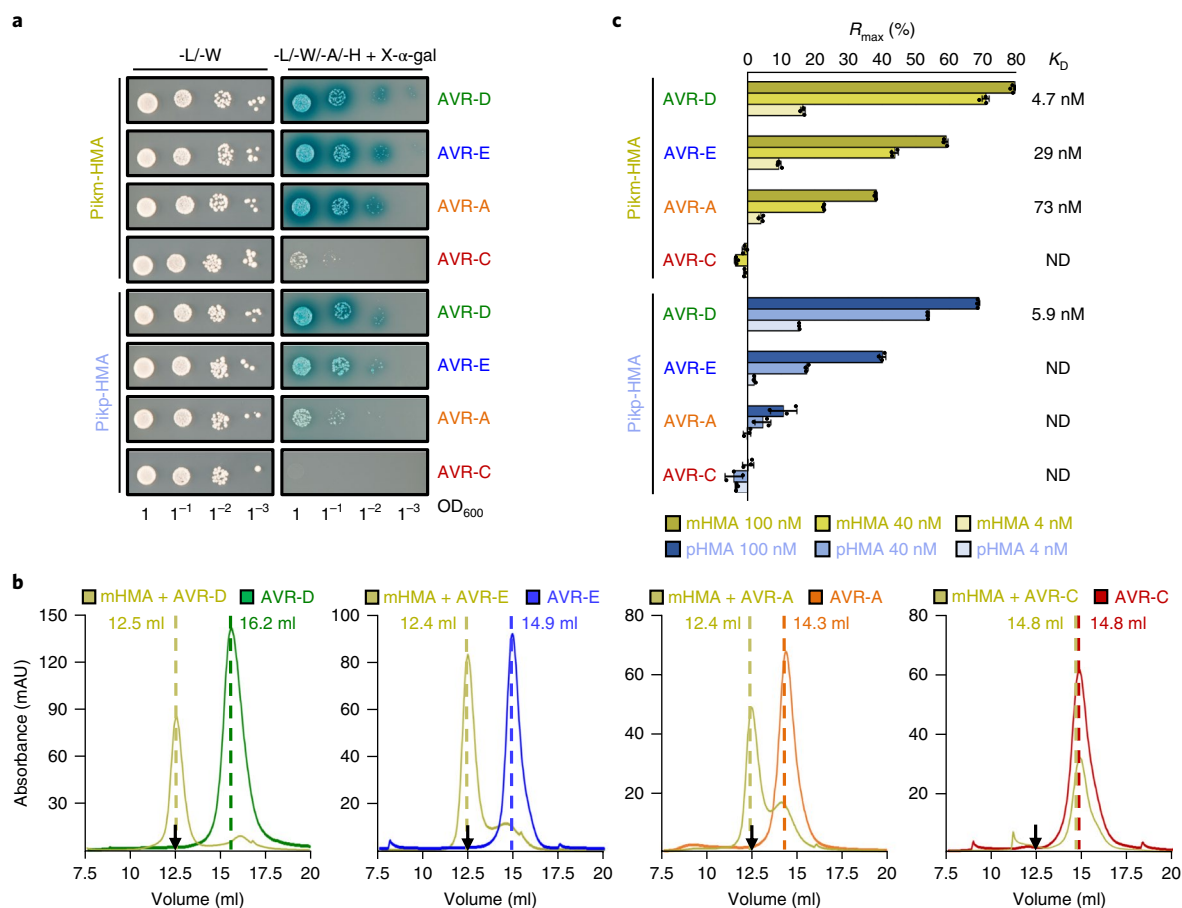


Fig. 2 | Different affinities underpin the recognition and response of Pik NLR alleles to AVR-Pik effector variants. **a**, Y2H demonstrates the binding of effector variants to both Pikm-HMA and Pikip-HMA. The control plate for yeast growth is on the left, with the selective plate on the right. Each experiment was repeated a minimum of three times, with similar results. **b**, Analytical gel filtration confirms that Pikm-HMA (mHMA) forms complexes with AVR-PikD, AVR-PikE and AVR-PikA in vitro, but not with AVR-PikC. Note that earlier elution correlates with increased molecular mass. The retention volumes for peaks are labelled (the black arrow indicates the Pikm-HMA elution volume; Pikm-HMA does not absorb light at 280 nm). SDS-PAGE with relevant fractions are shown in Supplementary Fig. 2b. Each experiment was repeated a minimum of three times, with similar results. **c**, SPR reveals that the in vitro binding affinity between Pik-HMA and effectors correlates with in planta responses. R_{max} (%) is the percentage of the theoretical maximum response, assuming a 1:1 binding model for Pikm (effector:HMA) and a 1:2 binding model for Pikip, at the HMA concentrations shown. Bars represent the average of three measurements, and the error bars represent the standard deviation. Where K_D values are given, a wider range of HMA concentrations were used for this calculation (see Supplementary Fig. 2c–e.g). pHMA, Pikip-HMA; ND, not determined.

shown previously³³ (Supplementary Fig. 1a,b). The expression of each protein was confirmed by western blot (Supplementary Fig. 1c).

Allele-specific effector responses in planta correlates with direct Pik-HMA interactions. We used yeast-2-hybrid (Y2H) to investigate whether the binding of effectors to the Pikip-HMA or Pikm-HMA correlates with in planta response profiles. We observed comparable growth of yeast on selective plates and the development of blue colouration with X- α -gal (which are both indicative of protein–protein interactions) with Pikm-HMA and AVR-PikD, AVR-PikE and AVR-PikA, but not with AVR-PikC (Fig. 2a). Although the Y2H assay with Pikip-HMA or Pikip-HMA showed comparable interaction with AVR-PikD, Pikm-HMA showed increased interaction with AVR-PikE and markedly stronger interaction with AVR-PikA (Fig. 2a). No growth was observed with Pikip-HMA and AVR-PikC. All proteins were confirmed to be expressed in yeast (Supplementary Fig. 2a).

Pikm-HMA has tighter binding affinities for AVR-Pik effectors than Pikip-HMA in vitro. To produce stable Pikm-HMA protein for in vitro studies, we cloned a construct with a 5-amino

acid extension at the C terminus (encompassing residues Gly 186–Asp 264 of the full-length protein) compared to the previously studied Pikip-HMA³³. Using gel filtration with separately purified proteins, Pikm-HMA forms complexes with the effectors AVR-PikD, AVR-PikE or AVR-PikA, but not with AVR-PikC (Fig. 2b and Supplementary Fig. 2b).

To determine the extent to which the expanded response of Pikm to AVR-Pik effectors in *N. benthamiana* is related to the strength of binding to the Pikm-HMA, we determined binding affinities by surface plasmon resonance (SPR). We monitored the response units following Pikm-HMA injection after capturing effectors on the chip surface. Binding of Pikm-HMA to the different effectors was measured at three different concentrations, and the response units were normalized to R_{max} (a theoretical maximum response, assuming a 1:1 interaction model). From this, we ranked the order of apparent affinity from highest to lowest (Fig. 2c). We then extended the Pikm-HMA concentration range to enable the estimation of the equilibrium dissociation constant (K_D). Using a 1:1 kinetics interaction model, we found that Pikm-HMA bound to AVR-PikD with the highest affinity (lowest K_D), followed by AVR-PikE and AVR-PikA (Fig. 2c, Supplementary Fig. 2c–e and Supplementary Table 1).

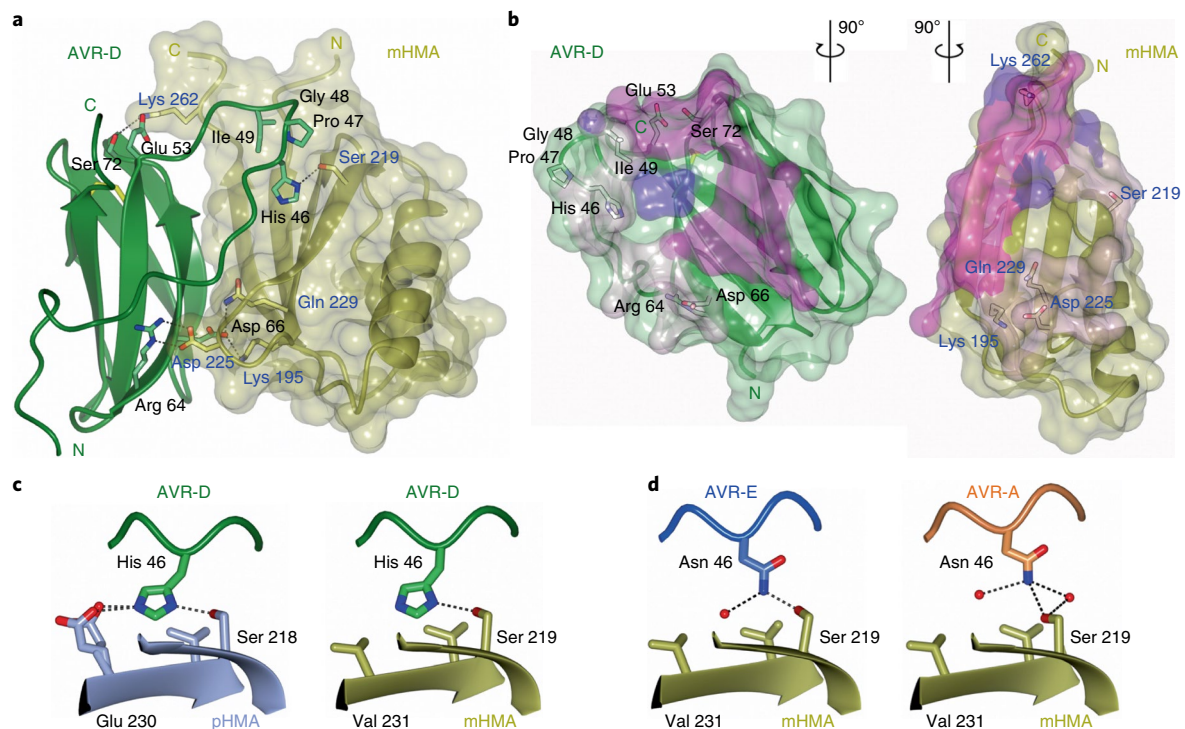


Fig. 3 | Structures of Pikm-HMA in complex with AVR-Pik effectors. a, Schematic representation of the structure of Pikm-HMA (mHMA) in complex with AVR-PikD. Pikm-HMA is shown with the selected side chains as sticks; the molecular surface of this domain is also shown. AVR-PikD is shown with the selected side chains as sticks. Hydrogen bonds or salt bridges are shown as dashed lines and the disulfide bond as a yellow bar. Amino acids labelled in black are from AVR-D, those labelled in blue are from mHMA. **b**, The buried surface area of AVR-PikD and Pikm-HMA shown from the perspective of the partner (the change in orientation from panel **a** is indicated). The buried surfaces are coloured according to interfaces described in the text (interface 1 is in purple, interface 2 is in pink and interface 3 is magenta). **c**, Close-up views (part of interface 2) of the orientation and interactions of AVR-PikD (His 46) in the Pikp-HMA (pHMA) and Pikm-HMA complexes. **d**, Close-up views (part of interface 2) of the orientation and interactions of AVR-PikE (Asn 46) (left panel) and AVR-PikA (Asn 46) (right panel) in complex with Pikm-HMA. Water molecules are shown as red spheres.

We observed no significant binding of Pikm-HMA to AVR-PikC (Fig. 2c, Supplementary Fig. 2f and Supplementary Table 1).

We also produced Pikp-HMA with its equivalent 5-amino acid C-terminal extension (including residues Gly 186–Asp 263 of the full-length protein) and analysed effector binding by SPR (Fig. 2c). We ranked effector-binding affinities in the order AVR-PikD > AVR-PikE > AVR-PikA (with no significant binding to AVR-PikC and assuming a 1:2 (effector:Pikp-HMA) interaction model, as previously observed³³). However, we were only able to reliably determine the K_D for Pikp-HMA bound to AVR-PikD (Fig. 2c and Supplementary Fig. 2g), as the binding of AVR-PikE and AVR-PikA were of insufficient quality under our assay conditions to allow the K_D to be determined (Supplementary Fig. 2h,i).

Based on these results and the interactions monitored by Y2H, we conclude that the differential binding affinity to the HMA domains is the source of the allele-specific response profile in *N. benthamiana* and of rice cultivars to *M. oryzae* strains expressing AVR-Pik variants³⁴.

Structures of Pik-HMAs in complex with AVR-Pik effectors reveal multiple interaction surfaces. Using a co-expression strategy, we obtained complexes of Pikm-HMA bound to AVR-PikD, AVR-PikE or AVR-PikA. Each of these were crystallized and X-ray diffraction data were collected at the Diamond Light Source (Oxford, UK) to 1.2-Å, 1.3-Å and 1.3-Å resolution, respectively. Details of the X-ray data collection, structure solution and structure completion are given in the Methods section and Supplementary Table 2. The overall orientations of each component in the Pikm-HMA–effector complexes are similar to each other and to the

previously determined Pikp-HMA–AVR-PikD structure³³ (Fig. 3a, Supplementary Fig. 3a,b and Supplementary Table 3). Interestingly, the Pikm-HMA–effector structures form a 1:1 complex, in contrast to Pikp-HMA–AVR-PikD, which formed a 2:1 complex³³. Pikp-HMA dimerization is most likely an artefact of in vitro protein expression and purification.

Analysis of the interfaces formed between Pikm-HMA and the effectors using QtPISA³⁶ (Supplementary Table 4 and Supplementary Fig. 4) reveals they are broadly similar to each other, although there is a trend of reducing the total interface area in the order AVR-PikD > AVR-PikE > AVR-PikA. Graphical representation of key interface components (using QtPISA interaction radars³⁶; Supplementary Fig. 4) reveals a high likelihood that each interface is biologically relevant: each key component value lies well above the 50% threshold when considered against statistical distributions derived from the Protein Data Bank (PDB) (see Methods and ref.³⁶).

Three predominant regions can be identified within each Pikm-HMA–effector interface (Figs. 1c and 3b). These regions (interfaces) are defined here from the HMA side as: interface 1, amino-terminal residues Glu 188–Lys 191; interface 2, residues from β -2 to β -3 (Ser 219–Val 233) and Lys 195 from β -1; and interface 3, residues from β -4 to the C terminus (Met 254–Asp 264) (Figs. 1c and 3b).

Interface 1 is a minor component of the Pikm-HMA–effector interaction, with a single, weak hydrogen bond formed by the side chain of Lys 191 (to the main-chain carbonyl group of Thr 69 of the effector) and a hydrophobic interface contributed by the side chain of Met 189 (to the side chain of Ile 49 of the effector). Interface 2 is more extensive and predominately interacts with AVR-Pik residues from the N-terminal extension of the conserved MAX effector fold³⁷,

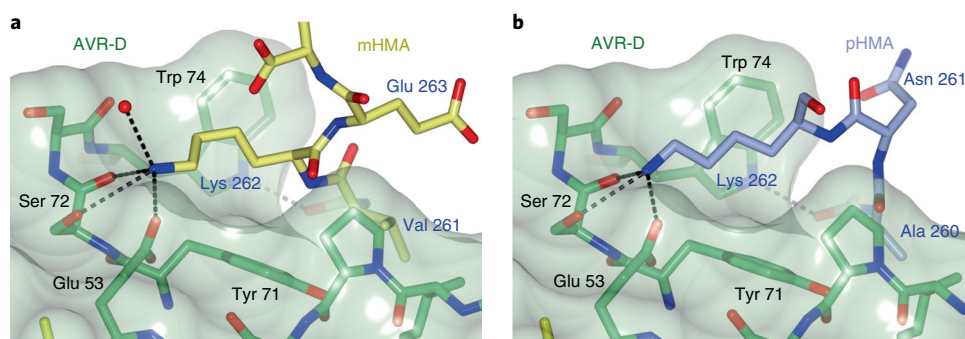


Fig. 4 | Different interactions at interface 3 in the complexes of Pikm-HMA and Pikp-HMA with AVR-PikD support recognition and response.

A close-up view of the interactions across interface 3 in the Pikm-HMA (mHMA; **a**) and Pikp-HMA (pHMA; **b**) complexes with AVR-PikD, showing different conformations for the C-terminal regions of the HMA domains. In particular, note the looping out of Asn 261 of Pikp-HMA (**b**) and the different orientation of the Lys 262 side chain (**a,b**). In each panel, AVR-PikD is shown with the side chains as sticks; the molecular surface of the effector is also shown. The Pik-HMA domains are coloured as labelled.

including Arg 39–Phe 44 and His 46–Ile 49. This interface includes the polymorphic residues at positions 46, 47 and 48 of the effector variants³⁴ (Figs. 1b and 3). Interface 2 also includes salt-bridge or hydrogen-bond interactions via the side chains of Asp 225 (to Arg 64 of the effectors) and Lys 195 (to Asp 66 of the effectors; Fig. 3a). Finally, interface 3 includes both main-chain hydrogen-bonding interactions between β -4 of the HMA and β -3 of the effectors, and inserts the side chain of Lys 262 into a surface pocket on the effector lined by residues Glu 53, Tyr 71, Ser 72 and Trp 74. Lys 262 makes several interactions in this pocket, including salt bridges or hydrogen bonds with the side chains of Glu 53 and Ser 72 (Figs. 3a and 4a).

We also obtained crystal structures of Pikp-HMA, with the 5-amino acid extension at the C terminus of the HMA, bound to AVR-PikD or AVR-PikE at 1.35-Å and 1.9-Å resolution, respectively (see Methods, Supplementary Table 2 and Supplementary Fig. 3c,d). The Pikp-HMA–AVR-PikE combination does not give rise to responses in planta, but we were able to obtain the complex in solution. The new structure of the Pikp-HMA–AVR-PikD complex is essentially identical to that previously determined³³, except for the 5-amino acid extension. Interface analysis with QtPISA (Supplementary Table 4 and Supplementary Fig. 4) reveals that the Pikp-HMA–AVR-PikD complex has broadly similar properties to those of Pikm-HMA–effectors (the total interface area and the key component values are well above the 50% threshold in the interaction radars). By contrast, although the Pikp-HMA–AVR-PikE interface shows a broadly similar total interface area to the other complexes, the total calculated binding energy is reduced (the area of the polygon in Supplementary Fig. 4) and five out of six key interface components fall below the 50% threshold, questioning the biological relevance of this interface.

Structural changes at interface 2 underpin differential effector recognition by Pikm. Effector variants AVR-PikD, AVR-PikE and AVR-PikA differ at amino acid positions 46, 47 and 48, which localize to interface 2 (Figs. 1b and 3b). Pikp-HMA binds to AVR-PikD (His 46) via hydrogen bonds with residues Ser 218 and Glu 230³³. In Pikm, the Ser is conserved, but Glu 230 is replaced by Val 231 at the structurally equivalent position, resulting in the loss of a direct hydrogen bond. Despite this, AVR-PikD (His 46) occupies the same position in both complexes (Fig. 3c). Surprisingly, in the Pikm-HMA–AVR-PikE complex, AVR-PikE (Asn 46) is rotated out of the binding pocket, well away from Val 231 (Fig. 3d), and a water molecule occupies the resulting space. Hydrogen bonds are formed between AVR-PikE (Asn 46:N δ 2) and both Pikm-HMA (Ser 219:OH) and the new water molecule. This configuration affects the position of effector residues Phe 44–Gly 48, pushing them away from the HMA domain, further altering interactions across

interface 2. These structural changes correlate with a reduced binding affinity of AVR-PikE with Pikm-HMA compared to AVR-PikD. In the Pikm-HMA–AVR-PikA complex, Asn 46 is rotated even further out of the HMA pocket, and, although a hydrogen bond is still formed with Pikm-HMA (Ser 219:OH), this is substantially different in orientation (Fig. 3d). These changes serve to move residues Asn 46–Pro 50 of AVR-PikA further away from the HMA domain, and again, these structural observations correlate with a reduced effector binding affinity. Interestingly, the polymorphic residues in AVR-PikA (Ala 47 and Asp 48) have no direct role in Pikm-HMA interaction. The polymorphisms in AVR-Pik do not significantly alter protein–protein interactions across interfaces 1 and 3, and these regions seem to stabilize the complexes.

We conclude that the structural changes at interface 2 underlie the weaker binding affinities of Pikm-HMA for AVR-PikE and AVR-PikA than for AVR-PikD.

Interactions across interface 3 contribute more to Pikm-HMA than to Pikp-HMA binding to AVR-PikD. As observed at interface 3 for the Pikm-HMA–effector complexes (Fig. 4a), a Lys residue from Pikp-HMA (Lys 262) locates to the binding pocket on the effector containing Glu 53 and Ser 72 (Fig. 4b). However, this Lys is shifted by one residue to the C terminus in the sequence of Pikp-1 (Fig. 1c). This results in a different conformation of the Pikp-HMA residues Ala 260 and Asn 261 when compared to Pikm-HMA (Val 261 and Lys 262), changing the interactions across interface 3. The most dramatic difference is the ‘looping out’ of Pikp-HMA (Asn 261) to retain Lys 262 in the effector-binding pocket (Figs. 4b and 5d,e), which affects the packing of Pikp-HMA (Ala 260) (Val 261 in Pikm-HMA) and the hydrophobic packing of the side chain of Lys 262.

Pik alleles also differ in the composition of residues at interfaces 1 and 2. Of most importance are the changes at interface 2 that contact AVR-PikD (His 46), as discussed above and in Fig. 3c.

We propose that Pikm has evolved more-robust interactions across interface 3 than Pikp to compensate for loss of binding, such as direct hydrogen bonds, at interface 2.

Interactions across interfaces 2 and 3 underpin the specificity of Pikp to AVR-PikD over AVR-PikE. Underpinning the global analyses of the Pikp-HMA–AVR-PikD and Pikp-HMA–AVR-PikE complexes are extensive differences at interfaces 2 and 3. At interface 2, AVR-PikE (Asn 46) is fully rotated out of the AVR-PikD (His 46) binding pocket (Fig. 5a–c). A hydrogen bond is still formed between AVR-PikE (Asn 46) and Pikp-HMA (Ser 218), but in a very different orientation (Fig. 5a–c). This results in residues Asn 46–Pro 50 moving away from the HMA domain. This re-configuration

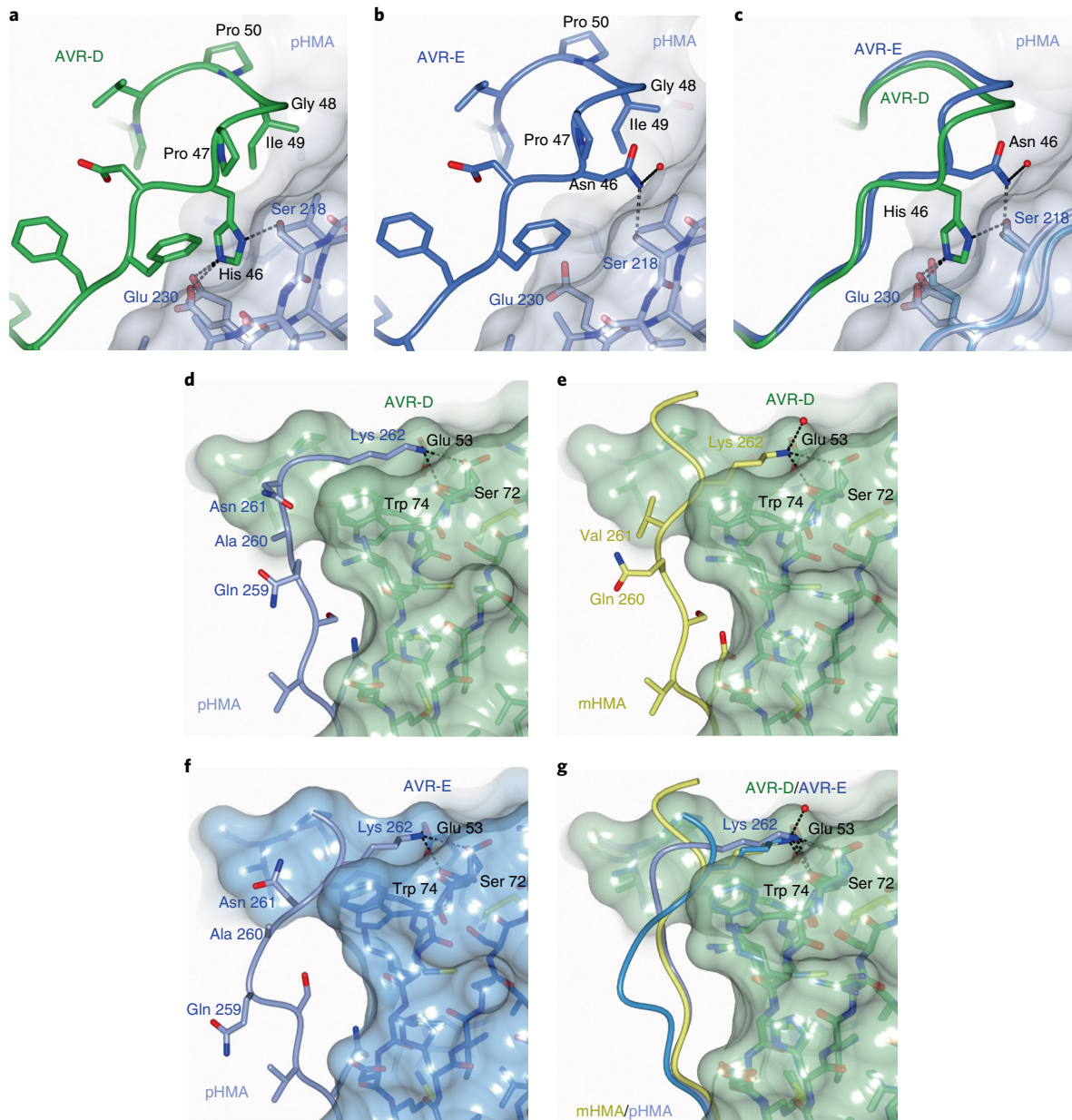


Fig. 5 | Altered interactions across the interfaces of Pikp-HMA with AVR-PikD and AVR-PikE underpin the differences in recognition and response.

a, b, Zoomed-in views of the interactions across interface 2 in the Pikp-HMA (pHMA) complexes with AVR-PikD (**a**) and AVR-PikE (**b**). In each panel, the molecular surface of Pikp-HMA is shown. Effector variant residues are coloured as labelled and shown in C- α -worm with side-chain representation. **c,** Superposition of panels **a** and **b**, with only selected side chains shown for clarity. The polymorphism at position 46 occupies a very different position, fully flipped out of the His 46 binding pocket in the AVR-PikE structure, which alters the position of residues Asn 44–Pro 50 relative to Pikp-HMA. **d–f,** Zoomed-in views of the interactions across interface 3 in the Pikp-HMA complex with AVR-PikD (**d**), the Pikm-HMA (mHMA) complex with AVR-PikD (**e**) and the Pikp-HMA complex with AVR-PikE (**f**). In each panel, the effector is shown as sticks and the molecular surface is also shown and coloured as labelled. Pik-HMA residues are coloured as labelled and shown in the C- α -worm with side-chain representation. The looping out of Asn 261 in Pikp compared to Pikm, when in complex with AVR-PikD, is seen in panels **d** and **e**, and the displacement of residues Gln 259 and Ala 260 in Pikp, between the complexes with AVR-PikD and AVR-PikE, is seen in panels **d** and **f**. **g,** Superposition of panels **d–f**, with only the side chain of Pik-HMA Lys 262 and only the surface of AVR-PikD, shown for clarity.

is coupled with changes at interface 3 (Fig. 5d,f,g). Interestingly, in the Pikp-HMA–AVR-PikE complex, Lys262 adopts a similar orientation to that found in the Pikm-HMA complexes (Fig. 5e–g). However, to enable this, residues Ser 258–Asn 261 adopt a dramatically different position, by looping out residues Gln 259 and Ala 260 from their positions in the Pikm-HMA complex (Fig. 5e–g), with consequent effects on this interface.

We conclude that interface 2 is key for effector recognition by Pikp and, unlike for Pikm, interfaces 1 and 3 are not able to compensate to enable productive binding.

Mutations at separate interfaces have differential effects on Pik-HMA–effector interactions and immunity phenotypes. We subsequently tested whether mutations in the effectors at interfaces 2

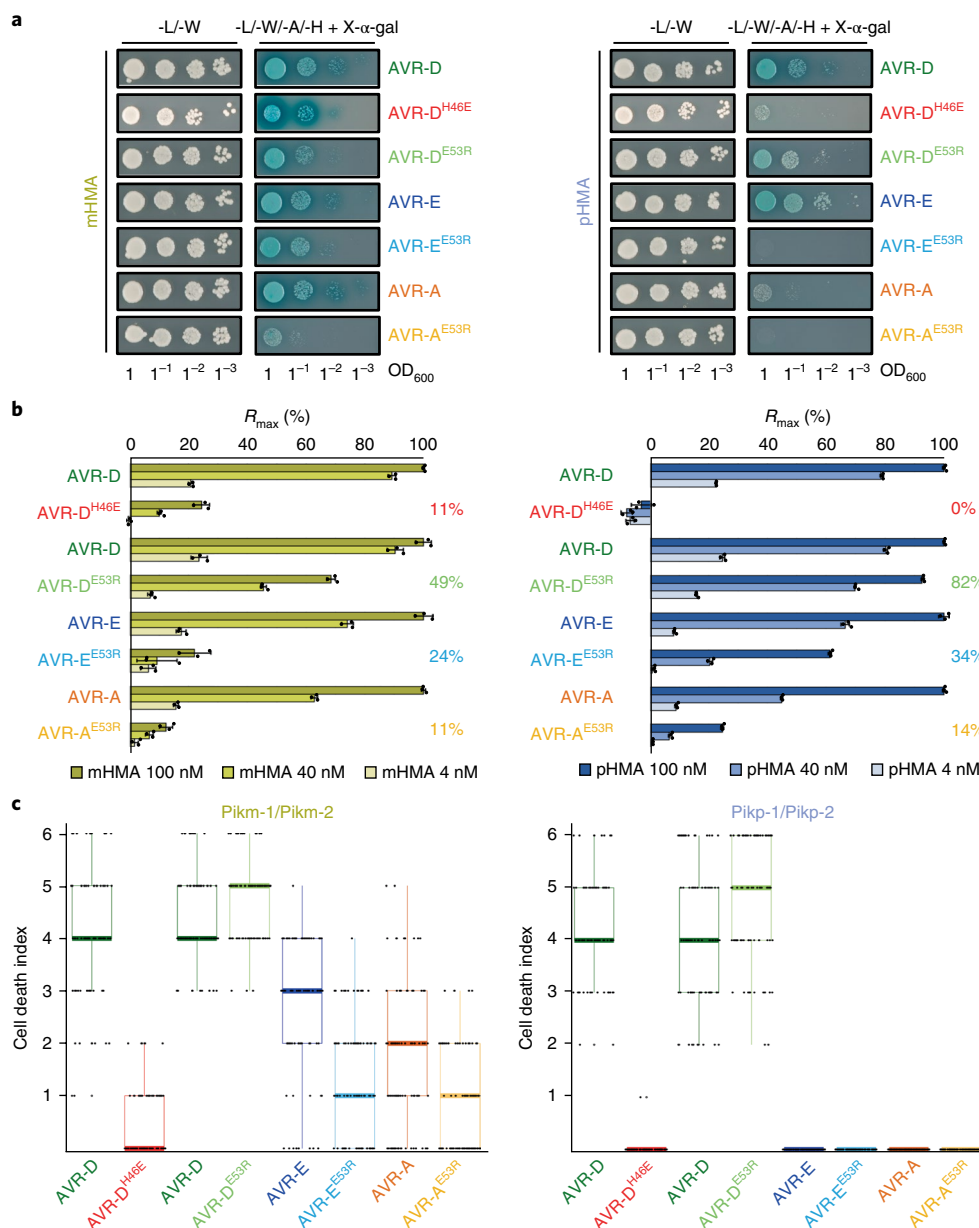


Fig. 6 | Mutations at different interfaces in the Pik-HMA-effector complexes have differential effects on interactions and phenotypes. a, Effector mutations at positions 46 and 53 perturb interactions with Pikm-HMA (mHMA) and Pikp-HMA (pHMA) as assayed by Y2H. Each experiment was repeated a minimum of three times, with similar results. Single-letter amino acid codes are shown. **b**, Changes in in vitro binding for effector mutants with Pikm-HMA and Pikp-HMA, as measured by SPR. The R_{max} (%) was calculated as described in the text. To emphasize the altered binding for each effector mutant, the averaged difference R_{max} (%) across the three different concentrations measured is shown. Bars represent the average of three measurements, with the error bars representing the standard deviation. **c**, Box plots of Pikm-mediated or Pikp-mediated cell death triggered by the effector mutants. For each sample, the number of repeats was 90. The centre line represents the median, the box limits are the upper and lower quartiles, the whiskers are the 1.5 \times interquartile range and all of the data points are represented as dots.

and 3 have differential effects on Pik-HMA binding and responses by Y2H, SPR and *N. benthamiana*. We used the previously characterized AVR-PikD (His46Glu) mutant at interface 2 and a Glu53Arg mutant at interface 3 in AVR-PikD, AVR-PikE and AVR-PikA. Although AVR-PikD (His46) occupies a central position at interface 2, AVR-Pik (Glu53) locates to the Pik-HMA (Lys262)-binding pocket, at the periphery of interface 3.

As previously observed (although without the C-terminal extension³³), the AVR-PikD (His46Glu) mutant essentially blocks the Pikp-HMA-effector interaction in Y2H and SPR, and abolishes Pikp-mediated cell death in *N. benthamiana* (Fig. 6a–c and

Supplementary Fig. 5). Interestingly, the AVR-PikD (His46Glu) mutant interacts with Pikm-HMA in Y2H (Fig. 6a). However, when measured by SPR, Pikm-HMA binding to this mutant is reduced to ~11% compared to the wild type (Fig. 6b). This reduction of binding in vitro is reflected in *N. benthamiana*, where we observe weak AVR-PikD (His46Glu)-dependent Pikm cell death (Fig. 6c and Supplementary Fig. 5b–d).

For each of the Glu53Arg effector mutants, we observe little effect on Pikm-HMA interaction in Y2H compared to the wild type, except a reduced interaction of AVR-PikA (Glu53Arg) (Fig. 6a). Interestingly, the Glu53Arg mutant in AVR-PikE abolishes the interaction of this

Table 1 | The various interactions and phenotypes between Pik NLR alleles and effector variants in this study

		AVR-D	AVR-E	AVR-A	AVR-C	AVR-D ^{H46E}	AVR-D ^{E53R}	AVR-E ^{E53R}	AVR-A ^{E53R}
Interaction in Y2H	Pikp	+++	++	+	–	+	++	–	–
	Pikm	+++	+++	+++	+	+++	++	++	+
Interaction in SPR	Pikp	+++	++	+	–	–	+++	+	–
	Pikm	+++	+++	++	–	+	++	+	–/+
Recognition in rice plants	Pikp	+++ ^a	+ ^a	– ^b	– ^b	– ^a	ND	ND	ND
	Pikm	+++ ^b	+++ ^b	+++ ^b	– ^b	ND	ND	ND	ND
CD response in <i>N. benthamiana</i>	Pikp	+++	–	–	–	–	+++	–	–
	Pikm	+++	++	+	–	+	+++	+	+

SPR and Y2H interactions used the isolated HMA domains, and in planta experiments were performed with full-length proteins. Recognition in rice plant Pikp is rice cv. K60. Recognition in rice plant Pikm is rice cv. Tsuyukake. CD, cell death; ND, not determined. ^aSee ref.³³. ^bSee ref.³⁴.

effector with Pikp-HMA in Y2H. Using SPR, the AVR-Pik (Glu53Arg) mutants show reduced binding to both Pik-HMA domains when compared pairwise to the wild type in each effector background (Fig. 6b). However, in each case, the Glu53Arg mutant has a greater effect in Pikm-HMA binding than in Pikp-HMA binding. Surprisingly, in the *N. benthamiana* cell death assay, we observe a slight increase in the AVR-PikD (Glu53Arg)-dependent cell death compared to the wild type for both Pikp and Pikm (Fig. 6c and Supplementary Fig. 5b–d). However, we see a reduction in the intensity of Pikm-mediated cell death for the effector variants AVR-PikE (Glu53Arg) and AVR-PikA (Glu53Arg) (Fig. 6c and Supplementary Fig. 5b–d).

We conclude that interactions across interface 2 are critical for effector recognition by Pikp and important for Pikm, and interface 3 has an important role in the extended response of Pikm to AVR-PikE and AVR-PikA.

Discussion

Despite intensive study, 25 years since the cloning of the first plant NLRs^{38–40}, very little is known about the molecular mechanistic basis of how these proteins recognize pathogen effectors and initiate immune signalling. The recent identification of plant NLRs with integrated domains^{28–30} has enabled new opportunities to investigate how these receptors directly recognize pathogen effectors at the biochemical and structural level, and how these binding events are linked to disease resistance^{33,41–44}. Here, we have generated five structures of different complexes between the integrated domains of an allelic NLR (Pik), and the variants of the effector (AVR-Pik) they recognize. When combined with the analysis of biophysical interactions in vitro and cell death responses in the model plant *N. benthamiana*, these structures provide new understanding, and unexpected findings, on how co-evolution has driven the emergence of new plant NLR receptor specificities.

High levels of diversifying selection in allelic plant NLRs and pathogen effectors suggest direct interaction between the proteins. Previous studies where structures of the effectors, but not the interacting NLR domain, were available showed that distributed surface-presented residues on the effectors defined NLR recognition specificity, mediated by polymorphic LRR domains^{14,15}. The integrated HMA domains are the most polymorphic regions of the rice Pik-1/Pik-2-paired NLRs, and Pik-HMA amino acids that form the interfaces with effectors are probably under the strongest selective pressure. Thus, during the course of plant–pathogen co-evolution, at least two alternative solutions for recognizing divergent effectors have emerged. One of these involves the integration and diversification of non-canonical domains in the NLR architecture. The second involves the diversification of LRR domains. An important question raised by these studies is what has driven the emergence of these different systems? An advantage of the integrated domain is that (once stably incorporated) it may tolerate the accelerated accumulation of

mutations, followed by selection for function, as mutations may be less likely to disrupt the overall structure and function of the NLRs.

One outcome from this work is the surprising plasticity of the Pik-HMA interfaces that supports differential recognition of AVR-Pik variants. Interactions across interface 2 are important for effector binding by Pikp-HMA and Pikm-HMA. Disruption of interface 2 by amino acid polymorphisms in AVR-PikE and AVR-PikA eliminates Pikp-mediated cell death in planta and weakens Pikm-mediated cell death. The unique polymorphism that defines AVR-PikC (Ala67Asp) also maps to interface 2 and may result in a steric clash preventing, or severely reducing, Pik-HMA binding. Our structural data support a conclusion that more-favourable interactions across interface 3 have evolved in Pikm-HMA to, in part, compensate for the effect of AVR-Pik variation at interface 2 and support cell death signalling. Our biophysical data indicate that quantitative binding differences, visualized as a disruption of interfaces in the structures, underpin differential effector recognition by Pik-HMAs and that a threshold of binding is required for the activation of response in planta. These insights will inform future structure–function studies to address whether rational engineering of Pik-HMA–effector-binding interfaces can generate NLR receptors with improved recognition profiles. Ultimately, we must understand how the recognition of effectors, through either integrated domains or other mechanisms, results in the triggering of immune responses in the context of the full-length proteins and, potentially, oligomeric states.

Methods

Gene cloning. For details of gene cloning, please see Supplementary Methods.

Expression and purification of proteins for in vitro binding studies. pOPINM, which encodes Pikm-HMA or Pikp-HMA, was transformed into *Escherichia coli* SHuffle cells⁴⁵. Inoculated cell cultures were grown in autoinduction media⁴⁶ at 30 °C for 6 h and 18 °C overnight. Cells were harvested and proteins were extracted as previously reported³³. AVR-Pik effectors with a cleavable N-terminal SUMO (small ubiquitin-like modifier) or MBP (maltose-binding protein) tag and a non-cleavable C-terminal 6×His tag were produced in and purified from *E. coli* SHuffle cells as previously described³³, using either autoinduction media⁴⁶ or Power Broth (Molecular Dimensions).

The protein concentration of AVR-Pik effectors was determined by absorption at 280 nm using a NanoVue spectrophotometer (GE Life Sciences). Measurements were corrected using the molar extinction coefficient 25,105 M^{–1} cm^{–1}, as calculated by ExPASy (<http://web.expasy.org/protparam>). Owing to the lack of aromatic residues in Pik-HMA, protein concentrations were measured using a Direct Detect Infrared Spectrometer (Merck).

Co-expression and purification of Pik-HMA–AVR-Pik effectors for crystallization. Relevant Pik-HMA domains and AVR-Pik effectors were co-expressed in SHuffle cells following co-transformation of pOPINM:Pik-HMA and pOPINA:AVR-Pik, as previously described³³. Cells were grown in autoinduction media (supplemented with both carbenicillin and kanamycin), harvested and processed as described in the Supplementary Methods. Protein concentrations were measured by absorbance at 280 nm using a NanoVue spectrophotometer

and an extinction coefficient of $25,105 \text{ M}^{-1} \text{ cm}^{-1}$ for Pikm-HMA complexes and $26,720 \text{ M}^{-1} \text{ cm}^{-1}$ for Pikip-HMA complexes, as calculated by ExPASy (<http://web.expasy.org/protparam>).

Protein–protein interaction. Analytical gel filtration. Pikm-HMA and the AVR-Pik effectors were mixed in a molar ratio of 2/1 and incubated on ice for 60 min. In each case, a sample volume of $110 \mu\text{l}$ was separated at 4°C on a Superdex 75 10/300 size exclusion column (GE Healthcare), pre-equilibrated in buffer B and at a flow rate of 0.5 ml min^{-1} . Fractions of 0.5 ml were collected for analysis by SDS–PAGE. The Superdex 75 10/300 column has a void volume of 7.4 ml and a total volume of 24 ml .

SPR. SPR experiments to analyse protein–protein interactions were performed on a Biacore T200 system (GE Healthcare) using an NTA sensor chip (GE Healthcare). All proteins were prepared in SPR running buffer (20 mM HEPES (pH 7.5), 860 mM NaCl and 0.1% Tween 20). Details of the cycling conditions are given in the Supplementary Methods.

The K_D for Pikm-HMA binding to AVR-Pik alleles and Pikip-HMA binding to AVR-PikD were determined from multicycle kinetics curves using the Biacore T200 BiaEvaluation software (GE Healthcare), with a 1:1 or 2:1 fit model, respectively. For the interaction between Pikip-HMA and AVR-PikE and AVR-PikA, and for both Pik-HMAs and the AVR-Pik mutants, it was not possible to accurately determine the K_D owing to the insufficient quality of the data. In these cases, the level of binding was expressed as a percentage of the R_{max} normalized for the amount of ligand immobilized on the chip. SPR data were exported and plotted using Microsoft Excel. Each experiment was repeated a minimum of three times, with similar results.

Y2H analyses. The Matchmaker Gold Yeast Two-Hybrid System (Takara Bio USA) was used to detect protein–protein interactions between Pik-HMAs and AVR-Pik effectors. The DNA encoding the Pik-HMAs in pGBKT7 was co-transformed with either the individual AVR-Pik variants or the mutants in pGADT7 into chemically competent *Saccharomyces cerevisiae* Y2HGold cells (Takara Bio USA). Single colonies grown on selection plates were inoculated in 5 ml SD^{-Leu-Trp} plate and grown overnight at 30°C . Saturated culture was then used to make serial dilutions of optical density at 600 nm (OD_{600}) 1 , 1^{-1} , 1^{-2} and 1^{-3} , respectively. Of each dilution, $5 \mu\text{l}$ was then spotted on a SD^{-Leu-Trp} plate as a growth control and also on a SD^{-Leu-Trp-Ade-His} plate containing X- α -gal and aureobasidine, as detailed in the user manual. Plates were imaged after incubation for 60 – 72 h at 30°C . Each experiment was repeated a minimum of three times, with similar results.

To confirm protein expression in yeast, the total protein was extracted from transformed colonies by boiling the cells for 10 min in LDS Runblue sample buffer. Samples were centrifuged, and the supernatant was subjected to SDS–PAGE before western blotting. The resulting membranes were probed with anti-GAL4 DNA-BD (Sigma) for the HMA domains in pGBKT7 and anti-GAL4 activation domain (Sigma) antibodies for the AVR-Pik effectors in pGADT7.

***N. benthamiana* cell death assays.** Transient gene expression in planta was performed by delivering T-DNA constructs with *Agrobacterium tumefaciens* GV3101 strain into 4-week-old *N. benthamiana* plants grown at 22 – 25°C with high light intensity. Pik-1, Pik-2, AVR-Pik and P19 were mixed at OD_{600} 0.4 , 0.4 , 0.6 and 0.1 , respectively. Detached leaves were imaged at 5 dpi from the abaxial side. Images are representative of three independent experiments, with internal repeats. The cell death index used for scoring is as presented previously³³ (also included in Supplementary Fig. 1d). The scoring for all replicates is presented as box plots, which were generated using R v3.4.3 (<https://www.r-project.org/>) and the graphic package ggplot2 (ref. ⁴⁷). The centre line represents the median, the box limits are the upper and lower quartiles, the whiskers are the $1.5\times$ interquartile range and all of the data points are represented as dots.

The presence of each protein, as expressed in representative assays, was determined by SDS–PAGE or western blot. For this, the leaf tissue was frozen and ground to fine powder in liquid nitrogen using a pestle and mortar. The leaf powder was mixed with two-times weight/volume ice-cold extraction buffer (10% glycerol, 25 mM Tris (pH 7.5), 1 mM EDTA, 150 mM NaCl, 2% w/v PVPP, 10 mM dithiothreitol, $1\times$ protease inhibitor cocktail (Sigma) and 0.1% Tween 20 (Sigma)), centrifuged at $4,200\text{g}$ at 4°C for 20 – 30 min and the supernatant was filtered ($0.45 \mu\text{m}$).

Crystallization, data collection and structure solution. For crystallization, Pik-HMA–AVR-Pik complexes were concentrated in buffer B (see Supplementary Methods). Sitting drop, vapour diffusion crystallization trials were set up in 96-well plates, using an Oryx nano robot (Douglas Instruments). Plates were incubated at 20°C , and crystals typically appeared after 24 – 48 h . For data collection, all crystals were harvested from the Morpheus HT-96 screen (Molecular Dimensions) and snap frozen in liquid nitrogen. The details of each crystallization condition are given in the Supplementary Methods.

X-ray data sets were collected at the Diamond Light Source. The data were processed using the xia2 pipeline⁴⁸ and AIMLESS⁴⁹, as implemented in CCP4⁵⁰. The structures were solved by molecular replacement using PHASER⁵¹ and the Pikip-HMA–AVR-PikD structure³³. The final structures were obtained through iterative

cycles of manual rebuilding and refinement using COOT⁵² and REFMAC5⁵³, as implemented in CCP4⁵⁰. Structures were validated using the tools provided in COOT and MOLPROBITY⁵⁴. More details on data collection and refinement are given in the Supplementary Methods.

Protein interface analyses. Protein interface analyses were performed using QtPISA⁵⁶. For each complex, one Pik-HMA–AVR-Pik effector assembly was used as a representative example. QtPISA interaction radars⁵⁶ were produced using the reference parameter ‘Total Binding Energy’. The area of the polygon indicates the likelihood of the interface to constitute part of a biological assembly (the greater the area, the more likely the interface constitutes part of a biological assembly). The scales along the beams compare the key interface properties to statistical distributions derived from the PDB. In general, if the radar area is contained within the 50% probability circle, then the interface is considered superficial and its biological relevance is questionable. In cases where the radar area is expanded outside the 50% probability circle, the interface is considered more likely to be significant and biologically relevant⁵⁶.

Reporting Summary. Further information on experimental design is available in the Nature Research Reporting Summary linked to this article.

Data availability. The coordinates and structure factors have been deposited in the PDB with accession codes 6FU9 (Pikm-HMA–AVR-PikD), 6FUB (Pikm-HMA–AVR-PikE), 6FUD (Pikm-HMA–AVR-PikA), 6G10 (Pikip-HMA–AVR-PikD) and 6G11 (Pikip-HMA–AVR-PikE).

Received: 26 February 2018; Accepted: 5 June 2018;
Published online: 09 July 2018

References

- Jones, J. D., Vance, R. E. & Dangl, J. L. Intracellular innate immune surveillance devices in plants and animals. *Science* **354**, aaf6395 (2016).
- Ronald, P. C. & Beutler, B. Plant and animal sensors of conserved microbial signatures. *Science* **330**, 1061–1064 (2010).
- Dodds, P. N. & Rathjen, J. P. Plant immunity: towards an integrated view of plant–pathogen interactions. *Nat. Rev. Genet.* **11**, 539–548 (2010).
- Win, J. et al. Effector biology of plant-associated organisms: concepts and perspectives. *Cold Spring Harb. Symp. Quant. Biol.* **77**, 235–247 (2012).
- Bialas, A. et al. Lessons in effector and NLR biology of plant–microbe systems. *Mol. Plant Microbe Interact.* **31**, 34–45 (2017).
- Ellis, J. G., Lawrence, G. J., Luck, J. E. & Dodds, P. N. Identification of regions in alleles of the flax rust resistance gene *L* that determine differences in gene-for-gene specificity. *Plant Cell* **11**, 495–506 (1999).
- Allen, R. L. et al. Host–parasite coevolutionary conflict between *Arabidopsis* and downy mildew. *Science* **306**, 1957–1960 (2004).
- Bhullar, N. K., Zhang, Z., Wicker, T. & Keller, B. Wheat gene bank accessions as a source of new alleles of the powdery mildew resistance gene *Pm3*: a large scale allele mining project. *BMC Plant Biol.* **10**, 88 (2010).
- Seeholzer, S. et al. Diversity at the *Mla* powdery mildew resistance locus from cultivated barley reveals sites of positive selection. *Mol. Plant Microbe Interact.* **23**, 497–509 (2010).
- Srichumpa, P., Brunner, S., Keller, B. & Yahiaoui, N. Allelic series of four powdery mildew resistance genes at the *Pm3* locus in hexaploid bread wheat. *Plant Physiol.* **139**, 885–895 (2005).
- Lu, X. et al. Allelic barley MLA immune receptors recognize sequence-unrelated avirulence effectors of the powdery mildew pathogen. *Proc. Natl Acad. Sci. USA* **113**, E6486–E6495 (2016).
- Dodds, P. N. et al. Direct protein interaction underlies gene-for-gene specificity and coevolution of the flax resistance genes and flax rust avirulence genes. *Proc. Natl Acad. Sci. USA* **103**, 8888–8893 (2006).
- Krasileva, K. V., Dahlbeck, D. & Staskawicz, B. J. Activation of an *Arabidopsis* resistance protein is specified by the in planta association of its leucine-rich repeat domain with the cognate oomycete effector. *Plant Cell* **22**, 2444–2458 (2010).
- Steinbrenner, A. D., Goritschnig, S. & Staskawicz, B. J. Recognition and activation domains contribute to allele-specific responses of an *Arabidopsis* NLR receptor to an oomycete effector protein. *PLoS Pathog.* **11**, e1004665 (2015).
- Wang, C. I. et al. Crystal structures of flax rust avirulence proteins AvrL567-A and -D reveal details of the structural basis for flax disease resistance specificity. *Plant Cell* **19**, 2898–2912 (2007).
- Huang, J., Si, W., Deng, Q., Li, P. & Yang, S. Rapid evolution of avirulence genes in rice blast fungus *Magnaporthe oryzae*. *BMC Genet.* **15**, 45 (2014).
- Raffaele, S. et al. Genome evolution following host jumps in the Irish potato famine pathogen lineage. *Science* **330**, 1540–1543 (2010).
- Yoshida, K. et al. Association genetics reveals three novel avirulence genes from the rice blast fungal pathogen *Magnaporthe oryzae*. *Plant Cell* **21**, 1573–1591 (2009).

19. Dangl, J. L., Horvath, D. M. & Staskawicz, B. J. Pivoting the plant immune system from dissection to deployment. *Science* **341**, 746–751 (2013).
20. Rodriguez-Moreno, L., Song, Y. & Thomma, B. P. Transfer and engineering of immune receptors to improve recognition capacities in crops. *Curr. Opin. Plant Biol.* **38**, 42–49 (2017).
21. Eitas, T. K. & Dangl, J. L. NB-LRR proteins: pairs, pieces, perception, partners, and pathways. *Curr. Opin. Plant Biol.* **13**, 472–477 (2010).
22. Wu, C. H., Belhaj, K., Bozkurt, T. O., Birk, M. S. & Kamoun, S. Helper NLR proteins NRC2a/b and NRC3 but not NRC1 are required for Pto-mediated cell death and resistance in *Nicotiana benthamiana*. *New Phytol.* **209**, 1344–1352 (2016).
23. Narusaka, M. et al. *RRS1* and *RPS4* provide a dual Resistance-gene system against fungal and bacterial pathogens. *Plant J.* **60**, 218–226 (2009).
24. Sinapidou, E. et al. Two TIR:NB-LRR genes are required to specify resistance to *Peronospora parasitica* isolate Cala2 in *Arabidopsis*. *Plant J.* **38**, 898–909 (2004).
25. Ashikawa, I. et al. Two adjacent nucleotide-binding site-leucine-rich repeat class genes are required to confer *Pikm*-specific rice blast resistance. *Genetics* **180**, 2267–2276 (2008).
26. Lee, S. K. et al. Rice *Pi5*-mediated resistance to *Magnaporthe oryzae* requires the presence of two coiled-coil-nucleotide-binding-leucine-rich repeat genes. *Genetics* **181**, 1627–1638 (2009).
27. Wu, C. H. et al. NLR network mediates immunity to diverse plant pathogens. *Proc. Natl Acad. Sci. USA* **114**, 8113–8118 (2017).
28. Cesari, S., Bernoux, M., Moncuquet, P., Kroj, T. & Dodds, P. N. A novel conserved mechanism for plant NLR protein pairs: the “integrated decoy” hypothesis. *Front. Plant Sci.* **5**, 606 (2014).
29. Kroj, T., Chanclud, E., Michel-Romiti, C., Grand, X. & Morel, J. B. Integration of decoy domains derived from protein targets of pathogen effectors into plant immune receptors is widespread. *New Phytol.* **210**, 618–626 (2016).
30. Sarris, P. F., Cevik, V., Dagdas, G., Jones, J. D. & Krasileva, K. V. Comparative analysis of plant immune receptor architectures uncovers host proteins likely targeted by pathogens. *BMC Biol.* **14**, 8 (2016).
31. Wu, C. H., Krasileva, K. V., Banfield, M. J., Terauchi, R. & Kamoun, S. The “sensor domains” of plant NLR proteins: more than decoys?. *Front. Plant Sci.* **6**, 134 (2015).
32. Okuyama, Y. et al. A multifaceted genomics approach allows the isolation of the rice *Pia*-blast resistance gene consisting of two adjacent NBS-LRR protein genes. *Plant J.* **66**, 467–479 (2011).
33. Maqbool, A. et al. Structural basis of pathogen recognition by an integrated HMA domain in a plant NLR immune receptor. *eLife* **4**, e08709 (2015).
34. Kanzaki, H. et al. Arms race co-evolution of *Magnaporthe oryzae* AVR-Pik and rice *Pik* genes driven by their physical interactions. *Plant J.* **72**, 894–907 (2012).
35. Costanzo, S. & Jia, Y. L. Sequence variation at the rice blast resistance gene *Pi-km* locus: implications for the development of allele specific markers. *Plant Sci.* **178**, 523–530 (2010).
36. Krissinel, E. Stock-based detection of protein oligomeric states in jsPISA. *Nucleic Acids Res.* **43**, W314–W319 (2015).
37. de Guillen, K. et al. Structure analysis uncovers a highly diverse but structurally conserved effector family in phytopathogenic fungi. *PLoS Pathog.* **11**, e1005228 (2015).
38. Bent, A. F. et al. *RPS2* of *Arabidopsis thaliana*: a leucine-rich repeat class of plant disease resistance genes. *Science* **265**, 1856–1860 (1994).
39. Mindrinos, M., Katagiri, F., Yu, G. L. & Ausubel, F. M. The *A. thaliana* disease resistance gene *RPS2* encodes a protein containing a nucleotide-binding site and leucine-rich repeats. *Cell* **78**, 1089–1099 (1994).
40. Whitham, S. et al. The product of the tobacco mosaic virus resistance gene *N*: similarity to toll and the interleukin-1 receptor. *Cell* **78**, 1101–1115 (1994).
41. Le Roux, C. et al. A receptor pair with an integrated decoy converts pathogen disabling of transcription factors to immunity. *Cell* **161**, 1074–1088 (2015).
42. Sarris, P. F. et al. A plant immune receptor detects pathogen effectors that target WRKY transcription factors. *Cell* **161**, 1089–1100 (2015).
43. Zhang, Z. M. et al. Mechanism of host substrate acetylation by a YopJ family effector. *Nat. Plants* **3**, 17115 (2017).
44. Ortiz, D. et al. Recognition of the *Magnaporthe oryzae* effector AVR-Pia by the decoy domain of the rice NLR immune receptor RGA5. *Plant Cell* **29**, 156–168 (2017).
45. Lobstein, J. et al. SHuffle, a novel *Escherichia coli* protein expression strain capable of correctly folding disulfide bonded proteins in its cytoplasm. *Microb. Cell Fact.* **11**, 56 (2012).
46. Studier, F. W. Protein production by auto-induction in high density shaking cultures. *Protein Expr. Purif.* **41**, 207–234 (2005).
47. Wickham, H. *ggplot. Elegant Graphics for Data Analysis* (Springer, New York, NY, 2009).
48. Winter, G. xia2: An expert system for macromolecular crystallography data reduction. *J. Appl. Crystallogr.* **43**, 186–190 (2010).
49. Evans, P. R. & Murshudov, G. N. How good are my data and what is the resolution? *Acta Crystallogr. D Biol. Crystallogr.* **69**, 1204–1214 (2013).
50. Winn, M. D. et al. Overview of the CCP4 suite and current developments. *Acta Crystallogr. D Biol. Crystallogr.* **67**, 235–242 (2011).
51. McCoy, A. J. et al. Phaser crystallographic software. *J. Appl. Crystallogr.* **40**, 658–674 (2007).
52. Emsley, P., Lohkamp, B., Scott, W. G. & Cowtan, K. Features and development of Coot. *Acta Crystallogr. D Biol. Crystallogr.* **66**, 486–501 (2010).
53. Murshudov, G. N. et al. REFMAC5 for the refinement of macromolecular crystal structures. *Acta Crystallogr. D Biol. Crystallogr.* **67**, 355–367 (2011).
54. Chen, V. B. et al. MolProbity: all-atom structure validation for macromolecular crystallography. *Acta Crystallogr. D Biol. Crystallogr.* **66**, 12–21 (2010).

Acknowledgements

This work was supported by the BBSRC (grants BB/J00453, BB/P012574 and BB/M02198X), the ERC (proposal 743165), the John Innes Foundation, the Gatsby Charitable Foundation and JSPS KAKENHI 15H05779. We thank the Diamond Light Source (beamlines I03 and I04 under proposals MX9475 and MX13467) for access to X-ray data collection facilities. We also thank D. Lawson and C. Stevenson (JIC X-ray Crystallography/Biophysical Analysis Platform) for help with protein structure determination and SPR.

Author contributions

J.C.D.I.C. and M.F. performed all of the experiments. J.C.D.I.C., M.F. and M.J.B. designed the experiments and analysed the data. A.M. and H.S. assisted with construct design and the initial protein production. R.T. and S.K. analysed the data. J.C.D.I.C., M.F. and M.J.B. wrote the manuscript with input from all authors.

Competing interests

The authors declare no competing interests.

Additional information

Supplementary information is available for this paper at <https://doi.org/10.1038/s41477-018-0194-x>.

Reprints and permissions information is available at www.nature.com/reprints.

Correspondence and requests for materials should be addressed to M.J.B.

Publisher's note: Springer Nature remains neutral with regard to jurisdictional claims in published maps and institutional affiliations.

Life Sciences Reporting Summary

Nature Research wishes to improve the reproducibility of the work that we publish. This form is intended for publication with all accepted life science papers and provides structure for consistency and transparency in reporting. Every life science submission will use this form; some list items might not apply to an individual manuscript, but all fields must be completed for clarity.

For further information on the points included in this form, see [Reporting Life Sciences Research](#). For further information on Nature Research policies, including our [data availability policy](#), see [Authors & Referees](#) and the [Editorial Policy Checklist](#).

Please do not complete any field with "not applicable" or n/a. Refer to the help text for what text to use if an item is not relevant to your study. [For final submission](#): please carefully check your responses for accuracy; you will not be able to make changes later.

▶ Experimental design

1. Sample size

Describe how sample size was determined.

No sample size calculation was performed. Sample size was based on previous literature and experimental logistic. The data is consistent within and between independent experiments.

2. Data exclusions

Describe any data exclusions.

No data were excluded.

3. Replication

Describe the measures taken to verify the reproducibility of the experimental findings.

SPR kinetic curves were measured at least 3 times using aliquots from at least 2 different protein preps, with comparable results.
For the cell death assay in *Nicotiana benthamiana* 3 biological replicas with 30 repeats each were performed. In the case of data shown in supplemental Fig.2 (repetition of previously published data with a different vector), one of the biological replicas included only 20 repeats. All attempt at replication were successful.
Co-IP and Yeast-2-Hybrid experiments were repeated at least 3 times with similar results.

4. Randomization

Describe how samples/organisms/participants were allocated into experimental groups.

No experimental group was used in this study. In the cell death assay, to avoid possible positional and developmental effect, each combination to be tested was spotted in a different position on the leaf, and on younger and older leaves, for each replica.

5. Blinding

Describe whether the investigators were blinded to group allocation during data collection and/or analysis.

No blinding has been used. High resolution images of all samples have been stored and could be scored again at any time.

Note: all in vivo studies must report how sample size was determined and whether blinding and randomization were used.

6. Statistical parameters

For all figures and tables that use statistical methods, confirm that the following items are present in relevant figure legends (or in the Methods section if additional space is needed).

- n/a Confirmed
- The exact sample size (*n*) for each experimental group/condition, given as a discrete number and unit of measurement (animals, litters, cultures, etc.)
 - A description of how samples were collected, noting whether measurements were taken from distinct samples or whether the same sample was measured repeatedly
 - A statement indicating how many times each experiment was replicated
 - The statistical test(s) used and whether they are one- or two-sided
Only common tests should be described solely by name; describe more complex techniques in the Methods section.
 - A description of any assumptions or corrections, such as an adjustment for multiple comparisons
 - Test values indicating whether an effect is present
Provide confidence intervals or give results of significance tests (e.g. P values) as exact values whenever appropriate and with effect sizes noted.
 - A clear description of statistics including central tendency (e.g. median, mean) and variation (e.g. standard deviation, interquartile range)
 - Clearly defined error bars in all relevant figure captions (with explicit mention of central tendency and variation)

See the web collection on [statistics for biologists](#) for further resources and guidance.

► Software

Policy information about [availability of computer code](#)

7. Software

Describe the software used to analyze the data in this study.

All crystallography data were processed using the CCP4 Program Suite v. 7.0.051 (including xia2, AIMLESS, COOT and REFMAC5) with user interface CCP4i2 v. 0.0.5 (<http://www.ccp4.ac.uk>).
The final models were evaluated using MOLPROBITY 4.4 (<http://molprobity.biochem.duke.edu>)
The boxplot were generated using R v. 3.4.3 (<https://www.r-project.org/>) and the graphic package ggplot2 (H. Wickham. ggplot2: Elegant Graphics for Data Analysis. Springer-Verlag New York, 2009).
All other graphs have been generated using Microsoft Excel for Mac v. 16.9 (Microsoft Corporation, USA)
The Surface Plasmon Resonance data were processed using the Biacore T200 Evaluation Software v. 2.0 from GE Healthcare Bio-Science AB, Sweden.

For manuscripts utilizing custom algorithms or software that are central to the paper but not yet described in the published literature, software must be made available to editors and reviewers upon request. We strongly encourage code deposition in a community repository (e.g. GitHub). [Nature Methods guidance for providing algorithms and software for publication](#) provides further information on this topic.

► Materials and reagents

Policy information about [availability of materials](#)

8. Materials availability

Indicate whether there are restrictions on availability of unique materials or if these materials are only available for distribution by a third party.

All unique materials used in this study are readily available from the authors.

9. Antibodies

Describe the antibodies used and how they were validated for use in the system under study (i.e. assay and species).

Anti c-Myc monoclonal antibody produced in mouse from Santa Cruz Biotechnology, Cat. n. c-Myc Antibody (9E10): sc-40 HRP, Lot n. A0716. Used diluted 1:3000.
 Monoclonal ANTI-FLAG® M2 antibody produced in mouse from SIGMA, Cat. n. F1804, Lot n. SLBT7654. Used diluted 1:3000.
 Monoclonal anti-HA high affinity antibody 3F10 produced in rat from Roche, Cat. n.11867423001, Lot.n. 14553800. Used diluted 1:3000.
 SIGMA Anti-GAL4 DNA-BD antibody produced in rabbit, Cat no. G3042. Used diluted 1:3000.
 SIGMA Anti-GAL4 Activation domain antibody produced in rabbit, Cat no. G9293. Used diluted 1:3000.
 Sigma Anti-Rat IgG-Peroxidase antibody produced in goat, Cat. no. A9307. Used diluted 1:10000
 SIGMA Anti-Rabbit IgG-Peroxidase antibody produced in goat, Cat. no. A0545. Used diluted 1:10000
 Promega Anti-Mouse IgG, HRP Conjugate, Cat. no. W4021. Used diluted 1:10000
 All the antibodies used in this study were commercial antibodies to standard epitope tags, validated by manufacturers.

10. Eukaryotic cell lines

a. State the source of each eukaryotic cell line used.

No eukaryotic cell lines have been used in this study.

b. Describe the method of cell line authentication used.

No eukaryotic cell lines have been used in this study.

c. Report whether the cell lines were tested for mycoplasma contamination.

No eukaryotic cell lines have been used in this study.

d. If any of the cell lines used are listed in the database of commonly misidentified cell lines maintained by [ICLAC](#), provide a scientific rationale for their use.

No eukaryotic cell lines have been used in this study.

► Animals and human research participants

Policy information about [studies involving animals](#); when reporting animal research, follow the [ARRIVE guidelines](#)

11. Description of research animals

Provide all relevant details on animals and/or animal-derived materials used in the study.

No animals were used in this study.

Policy information about [studies involving human research participants](#)

12. Description of human research participants

Describe the covariate-relevant population characteristics of the human research participants.

This study did not involved human research participants.